nature neuroscience

ARTICLES

Adult neural stem cells in distinct microdomains generate previously unknown interneuron types

Florian T Merkle[1–5,8], Luis C Fuentealba[1,2,8], Timothy A Sanders[1,2], Lorenza Magno[6,7], Nicoletta Kessaris[6,7,9] & Arturo Alvarez-Buylla[1,2,9]

Throughout life, neural stem cells (NSCs) in different domains of the ventricular-subventricular zone (V-SVZ) of the adult rodent brain generate several subtypes of interneurons that regulate the function of the olfactory bulb. The full extent of diversity among adult NSCs and their progeny is not known. Here, we report the generation of at least four previously unknown olfactory bulb interneuron subtypes that are produced in finely patterned progenitor domains in the anterior ventral V-SVZ of both the neonatal and adult mouse brain. Progenitors of these interneurons are responsive to sonic hedgehog and are organized into microdomains that correlate with the expression domains of the Nkx6.2 and Zic family of transcription factors. This work reveals an unexpected degree of complexity in the specification and patterning of NSCs in the postnatal mouse brain.

The mammalian ventricular-subventricular zone (V-SVZ) is a powerful model system for studying the processes of neurogenesis, migration and functional integration of newborn neurons. Each day, NSCs in the rodent V-SVZ produce thousands of interneurons that migrate to the olfactory bulb (OB), the brain region where olfactory information is first processed[1]. Continual interneuron turnover is essential for the maintenance of OB structure and olfactory discrimination[1–3].

Neurons derived from the postnatal V-SVZ mature into OB periglomerular cells (PGCs) or granule cells (GCs). PGCs can be further subdivided into three non-overlapping subtypes on the basis of the expression of calbindin, calretinin and tyrosine hydroxylase (CalB$^+$, CalR$^+$ and TH$^+$, respectively)[4]. GCs can be subdivided into four subtypes based on the location of their cell bodies in the intermediate (G_I), deep (G_{II}) or superficial (G_{III}) layers of the granule cell layer and their expression of CalR[5]. Each postnatally born neuron subtype plays a distinct role in the OB circuitry[6]. Our understanding of the full diversity of postnatally born interneuron types is incomplete, hampering efforts to understand the function of adult neurogenesis.

Adult-born OB neurons are produced by astrocyte-like NSCs (B1 cells) in the V-SVZ[7], an extensive germinal zone lining the postnatal lateral ventricle on its lateral wall and portions of its medial wall, extending rostrally along the rostral migratory stream (RMS) toward the OB core and dorsally and caudally into the subcallosal zone (reviewed in ref. 8). Recently, it has been recognized that different types of interneuron are produced in different subregions of the postnatal V-SVZ[9–12]. Defining the borders of these progenitor domains and identifying the cell types produced from each domain is a critical first step toward understanding the molecular mechanisms underlying neuronal subtype specification in the adult brain.

To explore the extent of diversity among NSCs and the cell types they produce, we mapped NSC progenitor domains in the newborn V-SVZ. We discovered new progenitor domains in the lateral ventricle that produce four previously unknown subtypes of postnatally born OB interneurons in both the newborn and adult brain. These cell types are generated from narrow microdomains patterned, in part, by the Nkx6.2 and Zic family of transcription factors (TFs), suggesting a functional role for these TFs in adult neurogenesis. The wide variety of cell types produced in such a small region highlights and extends the utility of the postnatal V-SVZ as a model system for studying the molecular mechanisms of neuronal subtype specification.

RESULTS

Identification of new OB interneuron subtypes

The spatial origin of different OB interneuron types has been studied by tracing the lineage of NSCs expressing regionally restricted TFs. However, since TF expression domains tend to be large and there is a limited repertoire of Cre recombinase–expressing mice that can be used for lineage tracing studies, this approach has limited power to uncover new stem cell populations. To complement TF-based lineage tracing, we previously developed a lineage tracing technique that takes advantage of the uniquely long basal process of radial glia, the principal NSC in embryonic and early postnatal brains (reviewed in ref. 13). These basal processes are readily infected by adenoviruses, which are then retrogradely transported to the radial glial cell body. Because adenoviral diffusion in the brain parenchyma is limited, this technique results in the infection of a small, spatially restricted patch of NSCs in the V-SVZ[9]. When an adenovirus expressing Cre

[1]Department of Neurological Surgery, University of California, San Francisco, San Francisco, California, USA. [2]Eli and Edythe Broad Center of Regeneration, Medicine and Stem Cell Research, University of California, San Francisco, San Francisco, California, USA. [3]Harvard Stem Cell Institute, Harvard University, Cambridge, Massachusetts, USA. [4]Department of Molecular and Cellular Biology, Harvard University, Cambridge, Massachusetts, USA. [5]Department of Stem Cell and Regenerative Biology, Harvard University, Cambridge, Massachusetts, USA. [6]Wolfson Institute for Biomedical Research, University College London, Gower Street, London, UK. [7]Department of Cell and Developmental Biology, University College London, Gower Street, London, UK. [8]These authors contributed equally to this work. [9]These authors jointly directed this work. Correspondence should be addressed to A.A.-B. (abuylla@stemcell.ucsf.edu).

Received 23 May; accepted 25 November; published online 22 December 2013; doi:10.1038/nn.3610

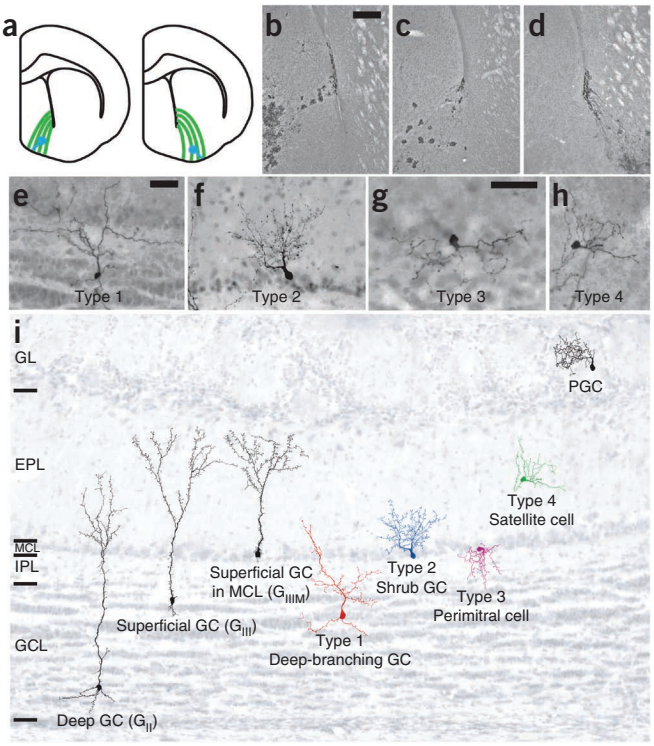

Figure 1 Production of type 1–4 cells in the OB by specifically labeled NSCs. (**a**) Radial glial cell targeting. Coronal representations of stereotaxic injections of small volumes of adenovirus infect cells locally at the injection site and needle tract (blue), as well as the long basal processes of radial glia (green), which transform into adult NSCs. (**b**–**d**) Diaminobenzidine (DAB)-stained photomicrographs of labeled cells in the P28 brain on the medial (**b**,**c**) and lateral (**d**) walls of the lateral ventricle. (**e**–**h**) Labeled NSCs in this region of the V-SVZ generated labeled type 1–4 OB cells, stained here by DAB. (**i**) Diagram showing camera lucida traces of previously known adult-born OB interneuron types (black) and newly identified cell types (red, blue, magenta, green) superimposed on a photomicrograph of a hematoxylin-stained OB to show their relative positions. Cells are shown to scale, and the pial surface is up. Scale bars represent 75 μm for **b**–**d** and 25 μm for **e**–**h**. GL, glomerular layer; GCL, granule cell layer.

recombinase (Ad:Cre) is injected into reporter mice that express GFP upon Cre-mediated recombination (Z/EG)[14], infected cells and their progeny become permanently labeled with GFP.

In this study, we labeled radial glial cells by injecting small volumes (20 nl) of Ad:Cre into the brains of postnatal day (P) 0 Z/EG mice and analyzed their progeny in the OB 28 d later by morphology and immunostaining for cell-type-specific markers. We targeted NSCs throughout the V-SVZ, including the subcallosal zone[15], dorsal[16] and medial walls[9] of the lateral ventricle, and the RMS[17] (reviewed in ref. 8). We observed labeled cells in the V-SVZ and the OB in 310 injected hemispheres. By varying the stereotaxic coordinates and angle of injection (**Fig. 1a**), we could reproducibly label different NSC populations along the medial and lateral walls of the lateral ventricle (**Fig. 1b**–**d**).

As previously reported, progenitors in the dorsal V-SVZ and subcallosal zone produced predominantly TH$^+$ PGCs and superficial GCs[9,11], and the RMS yielded large numbers of PGCs relative to other labeled OB cell types[9]. The ventral V-SVZ produced CalB$^+$ PGCs and deep GCs, as expected, but upon closer observation of brains containing anterior ventral V-SVZ labeling, we observed interneurons with distinctive morphologies that we had not seen before. We studied the morphology of these cells in detail using immunoperoxidase staining for GFP, which resulted in the Golgi stain–like filling of their cell bodies and fine processes. We identified four new interneuron subtypes with distinctive morphologies. These cell types had extensively branched dendritic arbors that frequently bore spines, characteristic of mature, functionally integrated neurons (**Figs. 1e**–**i**, **2** and **3** and **Supplementary Fig. 1**). In particular, their dendritic arbors and small cell bodies (approximately 6–7 μm/8–9 μm minor/major axis diameter) resembled those of OB interneurons, and a subset of them expressed the interneuron marker CalR (**Fig. 3** and **Supplementary Figs. 1** and **2**). We refer to these interneurons as type 1–4 cells.

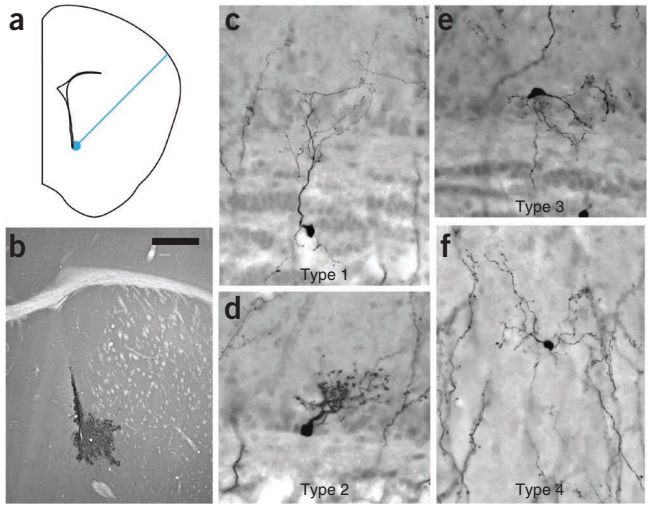

To determine whether these interneurons are also generated from adult NSCs, we stereotaxically injected Ad:GFAP-Cre into the ventral V-SVZ of P60 Z/EG mice. Ad:GFAP-Cre is an adenovirus that expresses Cre in GFAP$^+$ cells, so infected GFAP$^+$ cells and their progeny are specifically and permanently labeled in Cre reporter mice[9,18]. Upon Ad:GFAP-Cre injection, labeled cells in the V-SVZ were confined to the medial and lateral walls of the ventral tip of the V-SVZ (**Fig. 2a**,**b**). Twenty-eight days after viral injection, we observed type 1–4 cells in ten injected hemispheres that targeted the ventral V-SVZ (**Fig. 2c**–**f**) but not in 32 hemispheres that targeted the dorsal V-SVZ. We conclude that type 1–4 cells are generated in the adult ventral V-SVZ by GFAP$^+$ progenitors.

Characterization of type 1–4 cells

To further characterize type 1–4 cells, we examined their expression of known neurochemical markers. We did not observe any type 1–4 cells that expressed TH, somatostatin, parvalbumin or CalB. However, a substantial fraction of each cell type expressed CalR (**Fig. 3e** and **Supplementary Fig. 2**). The finding that type 1–4 cells are CalB$^-$ but CalR$^+$ confirms that these cells are distinct from the CalB$^+$ PGCs produced in the ventral V-SVZ[9,16].

Type 1 cells resembled GCs but were clearly distinct from previously characterized G_I, G_{II} or G_{III} cells[19]. In stark contrast to superficial

Figure 2 Type 1–4 cells continue to be produced by GFAP$^+$ NSCs in the adult anterior ventral V-SVZ. (**a**) Coronal diagram showing the injection tract (blue line) and injection site (blue circle) of Ad:GFAP-Cre targeting the anterior-ventral V-SVZ in a coronal schematic of the adult (P60) brain hemisphere (midline is to the left, dorsal is up). (**b**) DAB-stained photomicrograph of targeted V-SVZ and labeled striatal astrocytes 28 d after Ad:GFAP-Cre injection. (**c**–**f**) Type 1–4 cells can be identified by their distinctive morphologies in the OB 28 d after adult neural stem cell labeling. Scale bar represents 150 μm for **b**, 42 μm for **c**,**f** and 25 μm for **d**,**e**.

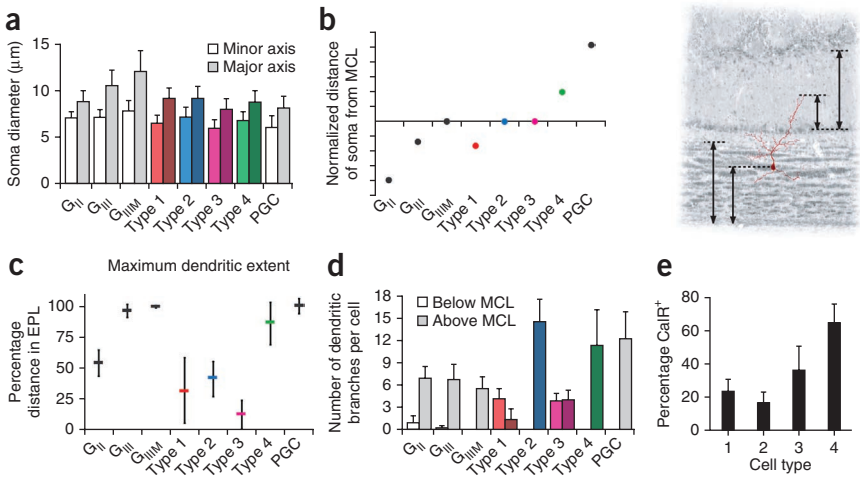

Figure 3 Molecular and morphological characterization of type 1–4 cells. (**a**) Cell body diameters measured along the minor and major axes for type 1–4 cells, GCs and PGCs. Abbreviations are as given in **Figure 1i**. (**b**) Quantification of mean soma position in the OB relative to the MCL normalized to the thickness of the GRL and EPL as diagrammed at right. Top and bottom tick marks correspond to the top of the EPL and OB core, respectively. (**c**) Maximum reach of the dendritic arbor into the EPL for each cell type. Although type 1 and 2 cells had superficially located cell bodies, their dendrites were restricted to the lower EPL, whereas superficial GCs (G_{III}, G_{IIIM}) consistently reached the most superficial EPL. (**d**) Analysis of the number of secondary and tertiary branches extending from the primary dendrite reveals a unique branching pattern that, along with other morphological characteristics, distinguishes type 1–4 cells from GCs and PGCs. (**e**) A subset of type 1–4 cells expressed CalR. Data are expressed as mean ± s.d. for **a**,**c**,**d** and mean ± s.e.m. for **e**. At least five mice were examined in each experimental group; see Source Data for numbers. Abbreviations for cell types and OB regions are given in **Figure 1** or the main text.

GCs (G_{III}), whose dendrites project near the top of the external plexiform layer (EPL), the dendrites of type 1 cells frequently failed to reach beyond the internal plexiform layer (IPL). Furthermore, whereas the dendrites of G_I, G_{II} or G_{III} cells branch primarily in the mitral cell layer (MCL) and EPL, the dendrites of this cell type branched primarily below the MCL in deeper regions of the OB (**Figs. 1i** and **3** and **Supplementary Fig. 1**). Following the naming convention of Shepherd and Greer[6], we call these cells deep-branching GCs (G_{IV}). Cells resembling deep-projecting GCs have previously been observed in the hamster and rabbit olfactory bulbs[20,21] but were not known to be generated postnatally.

Type 2 cells resembled GCs and had small, smooth cell bodies that lacked basal dendrites and were restricted to the MCL. These cells almost always extended only a single primary dendrite into the deep layer of the EPL. This dendrite branched extensively, giving rise to many small dendrites decorated with numerous spine-like protrusions, though the cells' arbors were spatially confined (**Figs. 1i** and **3** and **Supplementary Fig. 1**). On the basis of their distinctive shrub-like dendritic arbors, we call type 2 cells shrub GCs (G_V). Shrub cells have not been described in detail, but Blanes mentioned "tiny granule cells of the MCL"[22] that could correspond to type 2 cells.

The cell bodies of type 3 cells were confined to the MCL, from which they extended multiple thin, mostly spineless processes that branched both below and above the MCL and weaved tortuously in the MCL and IPL rather than being directed to the EPL (**Figs. 1i** and **3** and **Supplementary Fig. 1**). In some of these cells, immunoperoxidase staining revealed very lightly stained, fine processes extending straight up into the EPL that might correspond to axons. Because type 3 cells are located in the MCL and have dendritic arbors confined to this region, we call them perimitral cells (PMCs). PMCs are distinct from horizontal or vertical short axon cells, which have larger cell bodies (13–17 µm) and are usually found in the IPL[23].

Type 4 cells typically had cell bodies distributed throughout the EPL. To clearly distinguish them from type 3 cells and PGCs, we limited our analysis to cells separated by at least 100 µm from both the MCL and glomerular layer. The dendrites of type 4 cells were branched, were largely confined to the EPL, often projected radially and were decorated with varicosities but few spines (**Figs. 1i** and **3** and **Supplementary Fig. 1**). We occasionally observed a fine, lightly stained process, presumably an axon, that exited the cell body laterally and bifurcated radially. We identify type 4 neurons as satellite cells of the mouse main OB because they strongly resemble the satellite cells described in the main OB of hedgehogs[24] and the "dwarf" neurons of the rat accessory OB[25]. Satellite cells were clearly distinct from Van Gehuchten cells[26] (**Supplementary Fig. 2**), which were PV^+, had larger cell bodies (~13 µm) and were seen rarely after neonatal injections but never from adult injections.

GLI1$^+$ progenitors contribute to generation of type 1–4 cells

During embryogenesis, progenitor domains are set up by a combination of cell-intrinsic and cell-extrinsic factors acting on NSCs. V-SVZ progenitors likely maintain a cell-autonomous TF code, because they continue producing specific cell types when transplanted ectopically[9]. However, environmental factors may modulate this code, because activation of the sonic hedgehog (SHH) pathway is sufficient to partially respecify superficial GCs to deep GCs[27]. As the TF GLI1, a target gene of SHH, is highly expressed in the ventral V-SVZ, we hypothesized that SHH signaling in the ventral V-SVZ might contribute to type 1–4 cell specification. We therefore used *Gli1::CreER^{T2};R26-Ai14* mice[28] to identify OB neurons generated from *Gli1*$^+$ stem cells. In these mice, the *Gli1* promoter drives expression of CreER^{T2}, which translocates to the nucleus in the presence of tamoxifen[29] and excises a Stop cassette, activating a tdTomato reporter gene (**Fig. 4a**). We administered tamoxifen to both neonatal and adult mice (P0 and P30) (**Fig. 4b**). When we analyzed the brains of neonatal and adult mice 28 d after tamoxifen injection, we observed tdTomato-expressing (tdTomato$^+$) B1-like cells concentrated in the ventral V-SVZ (**Fig. 4c–e**). In the OB, we observed many labeled interneurons, including type 1–4 cells (**Fig. 4f**). These results indicate that at least some type 1–4 cells originate from SHH-responsive NSCs.

We next tested whether SHH activation is sufficient to ectopically specify type 1–4 cells by injecting Ad:Cre into *Rosa 26-Lox-Stop-Lox (LSL)-SmoM2;Ai14* neonatal mouse brains (**Fig. 4g**). In these mice, Ad:Cre infected radial glia and their progeny express SmoM2, a constitutively active mediator of SHH signaling[30]. When we targeted NSCs in the dorsal V-SVZ in *Ai14* control animals, we observed tdTomato$^+$ cells in the targeted region of the V-SVZ (**Fig. 4h**) and primarily superficial GCs and some PGCs in the OB (**Fig. 4i**). As previously described[27], tdTomato$^+$ GCs derived from SmoM2-expressing NSCs were shifted from a superficial to deep position in the GCL (**Fig. 4j**), confirming that SHH signaling was ectopically activated. However, we did not observe ectopic production of type 1–4 cells

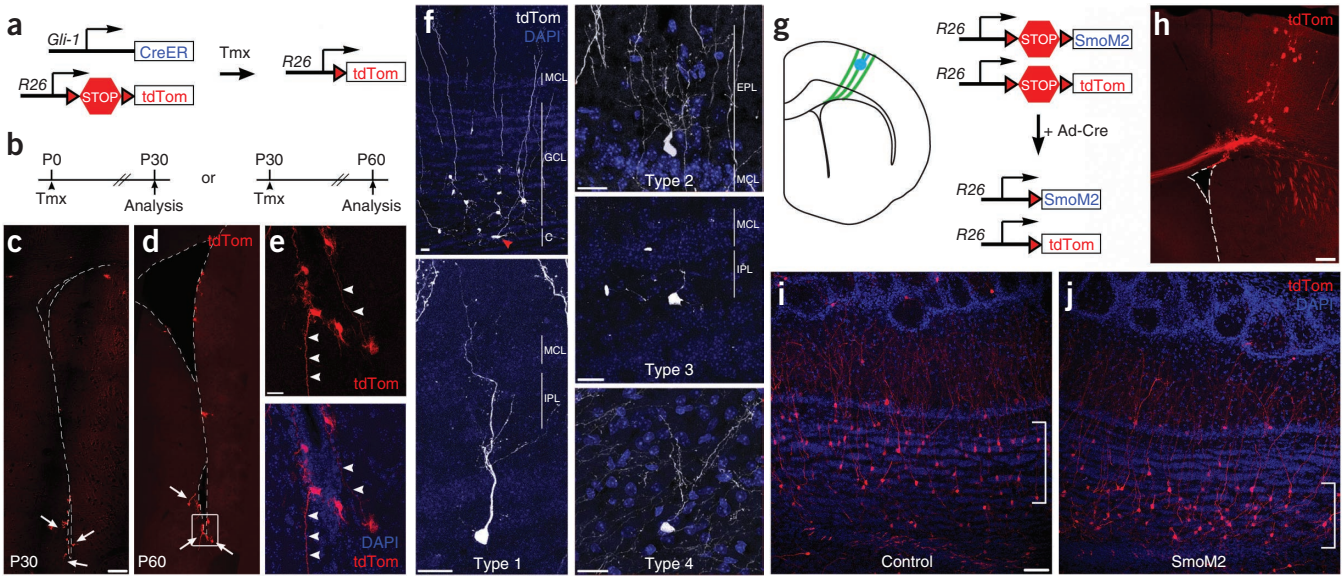

Figure 4 Gli1-expressing progenitors produce type 1–4 cells. (**a**) Diagram showing the *Gli1::CreER*^{T2} and *Rosa26-Ai14* alleles. tdTom, tdTomato; red triangles, *loxP* sites. (**b**) *Gli1::CreER*^{T2}*;Rosa26-Ai14* neonates (P0) and adult (P30) mice were treated with tamoxifen (Tmx) and analyzed 30 d later. (**c**–**e**) Coronal images. Most *Gli1*-expressing progenitors are located in the ventral V-SVZ in P30 (**c**) or P60 (**d**) animals (arrows) and frequently have B1 cell–like morphology with long basal processes (arrowheads, **e**). Dashed lines mark the ventricle (medial wall is on the left, lateral wall on the right). Panels in **e** are higher magnifications of the box shown in **d**. DAPI, 4′,6-diamidino-2-phenylindole. (**f**) *Gli1*$^{+}$ progenitors generate mainly deep GCs located close to the core of the OB at P30. Arrowhead (red) denotes a migrating neuroblast in the OB core (C). Type 1–4 cells are produced by *Gli1*-expressing progenitors. In these images, the tdTomato staining has been pseudocolored to improve its contrast. These are representative examples of type 1–4 cells observed from $n = 13$ mice. (**g**) Diagram showing the targeting of radial glia (green) in the cortical V-SVZ with Ad:Cre (blue) of a neonatal (P0) *Rosa26-LSL-SmoM2;Ai14* mouse brain. Upon Cre recombination, a constitutive active form of the Smo receptor (SmoM2) and tdTomato are expressed in cortical radial glia and their progeny. (**h**) Photomicrograph of a targeted *Rosa26-Ai14* brain section 28 d after Ad:Cre injection. (**i**,**j**) Cortical Ad:Cre injections in control *Rosa26-Ai14* neonates generated mostly superficial GCs (in brackets, **i**), while *Rosa26-LSL-SmoM2;Ai14* neonates produced deep GCs (in brackets, **j**), but no type 1–4 cells. These images are representative for each genotype of at least three independent experiments. Scale bars represent 120 μm for **c**,**d**, 20 μm for **e**,**f**, 200 μm for **h** and 60 μm for **i**,**j**.

from SmoM2-expressing dorsal progenitors among the tens of thousands of neurons we observed in the OB, indicating that, under the conditions we tested, the strong induction of SHH signaling was not sufficient to specify type 1–4 cells. These results suggest that other factors are required for type 1–4 cell specification. To identify these factors, we sought to define the borders of the type 1–4 cell progenitor domains and to test whether TFs expressed within these borders contribute to type 1–4 cell generation.

Progenitors of type 1–4 cells do not express Nkx2.1

To molecularly define the borders of type 1–4 cell progenitor domains, we first tested whether Nkx2.1^{+} progenitors contribute to type 1–4 cell production. Nkx2.1 is a candidate TF for type 1–4 cell specification because it is expressed in the embryonic medial ganglionic eminence (MGE) and ventral lateral ganglionic eminence (LGE)[31–34] and is maintained in late embryonic and early postnatal brains in the ventral tip of the V-SVZ[35,36]. Furthermore, lineage-tracing experiments have shown that Nkx2.1^{+} cells in the postnatal brain contribute to OB neurogenesis[12,37]. We first analyzed the spatial extent of Nkx2.1^{+} cells in neonatal and adult brains by immunofluorescence. We observed expression in the ventral tip of the V-SVZ starting at the level of the bed nucleus of the stria terminalis (bregma + 0.6 mm) (**Fig. 5d–f**) and extending caudally toward the anterior pretectal nucleus (bregma – 2.0 mm).

Next we used an inducible *Nkx2.1::CreER;Ai14* system[38] (**Fig. 5a**) to test whether postnatal *Nkx2.1*$^{+}$ progenitors give rise to type 1–4 cells. Because low numbers of OB neurons are derived from adult *Nkx2.1*$^{+}$ progenitors[12], we induced recombination in newborn *Nkx2.1::CreER*^{T2}*;Ai14* pups with daily injections of tamoxifen from P2–P6 and analyzed their brains at P34 (**Fig. 5b**). We observed many labeled cells in the V-SVZ and in the cerebral cortex of tamoxifen-injected animals, indicating efficient Cre-mediated recombination. The labeled cells we observed in the ventral V-SVZ were distributed in a pattern consistent with our immunostaining data (**Fig. 5c**). The cortical cells we observed might have been labeled by the persistent expression of the CreER^{T2} transgene in postmitotic cortical interneurons, or, as suggested by recent studies[35,39], they might be derived from the V-SVZ. Although we observed the production of OB GCs and PGCs upon *Nkx2.1::CreER*^{T2} lineage tracing (**Fig. 5g**,**h**), we never observed the generation of type 1–4 cells in tamoxifen-injected mice ($n = 10$). These results suggest that type 1–4 cells are likely generated in progenitor domains anterior to the broad *Nkx2.1* expression domain.

Nkx6.2^{+} progenitors contribute to type 1–4 cell generation

Nkx6.2 is another candidate TF that may define specific adult NSC populations. In the embryo, this TF is expressed in two small domains of the telencephalon: the interganglionic sulcus and the ventral septum[40]. Although its expression in the adult brain has not been described, Nkx6.2 is known to be a SHH-responsive gene and may thus be expressed in the postnatal brain in zones of high SHH activity. To determine whether this is the case and to identify *Nkx6.2*-derived OB neurons, we generated a *Nkx6.2::CreER*^{T2}*;Ai14* mouse line for *Nkx6.2* lineage tracing. First, we used *in situ* hybridization to confirm that *CreER*^{T2} expression was confined to the *Nkx6.2* expression domain. At embryonic day (E) 11.5, both *Nkx6.2* and *CreER*^{T2} were

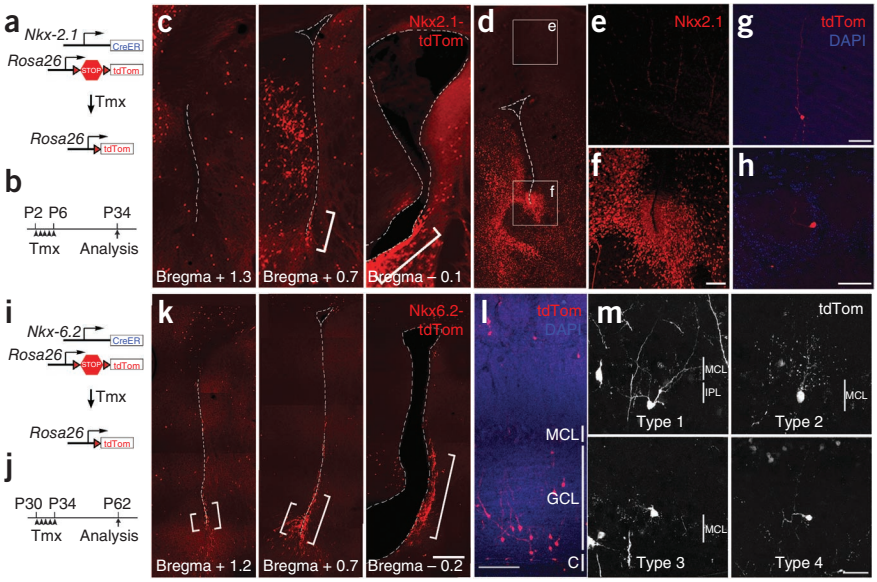

Figure 5 Type 1–4 cells are produced by postnatal progenitors expressing Nkx6.2, but not Nkx2.1. (**a**,**b**) Diagram showing the *Nkx2.1::CreER*^{T2} and *Rosa26-Ai14* alleles (**a**) and timing of tamoxifen (Tmx) administration and analysis (**b**). (**c**) *Nkx2.1* lineage-traced (tdTomato-expressing) cells are present in the ventral V-SVZ (brackets), shown here in coronal sections at different caudal-rostral levels. (**d**–**f**) Immunofluorescence for Nkx2.1 protein in the neonatal mouse brain showing strong Nkx2.1 expression in the ventral V-SVZ (near the bed nucleus of the stria terminalis in **d**,**f**) but no expression in the cortex (**d**,**e**). **e**,**f** are higher magnifications of the boxed areas in **d**. (**g**,**h**) *Nkx2.1*-expressing progenitors generate GCs (**g**) and PGCs (**h**) but not type 1–4 cells. (**i**,**j**) Diagram showing the *Nkx6.2::CreER*^{T2} and *Rosa26-Ai14* alleles (**i**) and timing of Tmx administration and analysis (**j**). (**k**) *Nkx6.2* lineage-traced cells with B1 cell–like morphology are present in the anterior ventral V-SVZ (brackets). (**l**) *Nkx6.2*$^{+}$ progenitors generate mainly deep GCs located close to the core (C) of the OB. (**m**) Type 1–4 cells are produced by *Nkx6.2*-expressing progenitors. In this image, the tdTomato staining has been pseudocolored to improve its contrast. Dashed lines mark the lateral ventricle walls (medial wall is on the left, lateral wall on the right) in **c**,**d**,**k**. Scale bars represent 60 μm for **f**–**h**, 200 μm for **l** and 25 μm for **m**. Scale bar in **k** represents 200 μm for **c**,**k**.

expressed in the ventral LGE and dorsal MGE, and at E15.5 their expression was confined to the medial and lateral walls of ventral tip of the V-SVZ (**Supplementary Fig. 3**).

To determine whether *Nkx6.2*$^{+}$ adult NSCs generate type 1–4 cells, we administered tamoxifen to reporter mice from P30–34 and analyzed labeled cells at P62 (**Fig. 5i,j**). In the adult V-SVZ, we observed a narrow and specific band of reporter gene expression in a region spanning the medial and lateral walls of the very ventral tip of the V-SVZ, extending from bregma + 1.5 mm to approximately bregma – 0.2 mm (**Fig. 5k**). In the olfactory bulb, we observed many labeled deep GCs, as expected (**Fig. 5l**). Notably, we also observed many examples of type 1, 2, 3 and 4 cells (1.8 ± 0.4% of all tdTomato^{+} cells, n = 4 mice; **Fig. 5m**). These data support the interpretation that type 1–4 cells continue to be produced in the adult brain by NSCs in a restricted domain in the anterior ventral V-SVZ where Nkx6.2 is expressed.

Zic^{+} progenitors contribute to a subset of type 1–4 cells

We next examined additional TFs expressed in the ventral V-SVZ that might contribute to the specification of type 1–4 cells. We focused on the zinc finger TF of the cerebellum (Zic) family for several reasons. First, *in situ* hybridization data show that Zic1 and Zic3 are sparsely expressed in the OB in the superficial granule cell layer, MCL and EPL, where type 1–4 cells are located[41]. Second, *Zic1*$^{-/-}$;*Zic3*$^{-/-}$ mice have smaller OBs, suggesting that Zic TFs regulate OB neurogenesis[41]. Third, Zic TFs are highly expressed in the septum (medial wall), but not in other brain regions known to contribute to the V-SVZ[42]. The septum is thought to developmentally contribute to the medial wall of the anterior V-SVZ, a region that may overlap with the progenitor domains for type 1–4 cells. For these reasons, we hypothesized that progenitors on the medial wall of the anterior ventral V-SVZ and their progeny in the OB might express Zic TFs.

To test this hypothesis, we characterized the Zic expression pattern in the adult OB and V-SVZ with an antibody that recognizes Zic1, Zic2 and Zic3 (refs. 43,44). The Zic protein expression pattern we observed in the OB (**Fig. 6a**) was consistent with existing *in situ* hybridization data. In the V-SVZ, Zic was expressed near the medial wall of the anterior ventral V-SVZ (**Fig. 6b** and **Supplementary Fig. 4**). Next, we asked whether Zic is expressed in the neurogenic lineage consisting of type B1 cells (GFAP^{+} NSCs), transit-amplifying type C cells and type A cells (neuroblasts)[45]. To aid in the morphological identification of these cells, we performed this analysis in Z/EG mice injected with Ad:Cre to target the medial or lateral wall of the anterior ventral V-SVZ. We found that Zic expression was barely detectable in a small subset of GFAP-expressing B1-like cells on the medial wall (**Fig. 6c**), but not on the lateral wall. Zic was clearly detectable in a subset of proliferative (5-ethynyl-2′-deoxyuridine (EdU)-incorporating and Ki67^{+}) type C–like cells on the medial wall (**Fig. 6e**,**f**), but not on the lateral wall. We also observed Zic in doublecortin (Dcx)-expressing type A–like cells on the medial wall of the V-SVZ, in the RMS and in the OB core (**Fig. 6d**,**g**). Together, these results suggest that Zic is upregulated in a subpopulation of type C and A cells derived from B1-like NSCs located in the medial wall of the anterior ventral V-SVZ. As Zic is also seen in a subset of OB interneuron types, we hypothesized that Zic might be maintained in at least some medially derived OB interneurons after they are born in the V-SVZ.

To test this hypothesis, we immunostained the OBs of Ad:Cre targeted mice for Zic. About 40% of PGCs produced by NSCs labeled in the medial wall of the anterior ventral V-SVZ were Zic^{+}, whereas almost no PGCs derived from the lateral wall were Zic^{+}. To extend this analysis to PGC subtypes, we co-stained PGCs for Zic and CalR, CalB or TH. While 39.5 ± 2.0% of CalR^{+} interneurons expressed Zic, only 2.5 ± 1.6% of CalB^{+} and 4.4 ± 1.3% of TH^{+} PGCs were Zic^{+} (**Fig. 6h**,**i** and **Supplementary Fig. 5**). This finding is consistent with the predominantly medial origin of CalR^{+} interneurons[9]. When we analyzed the Zic expression pattern of type 1–4 cells in the OB, we found that almost all type 1 and type 3 cells were Zic^{+}, whereas most type 2 or type 4 cells were immunonegative for Zic (**Fig. 6j**–**n**). Together, these studies identify Zic as a candidate molecular mediator for the specification of medially produced OB interneuron types and suggest that type 1 and 3 cells might be produced from Zic^{+} progenitor domains on the medial wall of

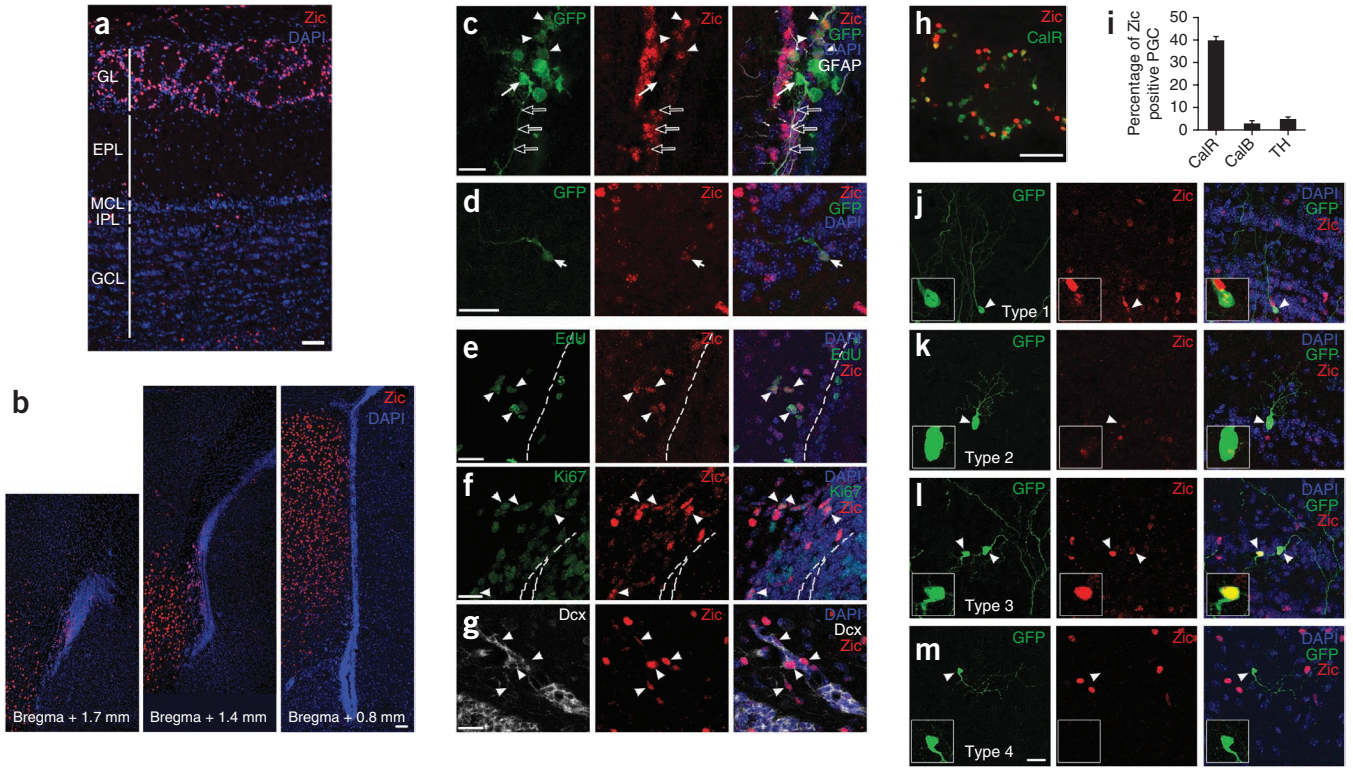

Figure 6 Expression of Zic proteins partitions type 1–4 production domains. (**a**) Zic expression in the OB, including the glomerular layer (GL), EPL, MCL, IPL and superficial granule cell layer (GCL). (**b**) Photomicrographs of coronal adult brain sections at three rostrocaudal levels showing Zic-immunopositive cells in the medial wall of the adult V-SVZ. (**c**,**d**) Zic expression in GFP$^+$ V-SVZ cell types derived from Ad:Cre-targeted radial glia in the medial V-SVZ. Zic is barely detectable in a small subpopulation of GFAP$^+$ B1 cells (closed arrow, B1 cell body; open arrows, basal process, in **c**). Zic is expressed in cells with morphologies characteristics of transit-amplifying cells (arrowheads in **c**) and migrating neuroblasts (in the RMS) (arrow in **d**). (**e**,**f**) Zic$^+$ proliferating progenitors in the medial V-SVZ incorporate EdU (1 h survival) (**e**) and express Ki67 (**f**). Dashed lines mark the lateral ventricle walls (medial wall is on the left, lateral wall on the right). Arrowheads denote colocalization of markers. (**g**) Within chains of migrating neuroblasts, Zic is expressed by a subpopulation of doublecortin (Dcx)$^+$ neuroblasts (arrowheads). (**h**) Colocalization of Zic and the OB interneuronal marker calretinin (CalR). Data are expressed as mean ± s.e.m. At least three mice per group were examined. (**i**) Quantification of CalR, CalB and TH expression in Zic$^+$ PGCs. (**j**–**m**) Most type 1 (**j**) and type 3 (**l**) cells express Zic protein, while type 2 (**k**) and type 4 (**m**) cells are mostly Zic negative. Insets represent higher magnifications of GFP$^+$ cells (arrowheads). (**n**) Quantification of Zic expression in type 1–4 cells. Data are presented as mean ± s.e.m., $n = 13$ mice. Quantifications and number of cells analyzed for **i**,**n** are provided in the Source Data. Scale bars represent 60 μm for **a**,**b**,**h** and 20 μm for **c**–**g**. Scale bar in **m** represents 20 μm for **j**–**m**.

the anterior ventral V-SVZ. This hypothesis could be addressed in future experiments by lineage tracing with Zic reporter mice.

Distinct microdomains partition the anterior ventral V-SVZ

To better define the borders of type 1–4 cell progenitor domains and complement our TF lineage-tracing data, we digitally traced the spatial extent of labeled V-SVZ cells in the 80 injected hemispheres that contained type 1–4 cells. We then aligned and overlaid these traces onto a common template to identify overlapping V-SVZ regions that consistently gave rise to these interneurons. This analysis identified a small region comprising the ventral tip (both medial and lateral walls) of the anterior lateral ventricle as a hot-spot for type 1–4 cell production (**Fig. 7a**,**b**). As expected, this region is rostral to the Nkx2.1 expression domain (bregma + 0.6 to 1.6 mm) but partially overlaps with the Zic expression domain and includes the rostral portion of the Nkx6.2 domain (**Fig. 7g**–**j**). When this region was specifically targeted with Ad:Cre, type 1–4 cells accounted for a substantial fraction (7.4 ± 2.9%, $n = 20$ mice) of labeled OB cells.

Next, we hypothesized that type 1–4 cells are produced in spatially distinct domains. A patch of labeled progenitors has a diameter of about 200 μm, which might span multiple small progenitor domains. Therefore, we selected the ten injections that generated the highest percentage of type 1 cells relative to all other labeled cells in the OB and identified the overlapping regions of labeled progenitors in the V-SVZ in these injections. By repeating this analysis for type 2–4 cells, we found that type 1 and type 3 cells were predominantly generated by radial glia labeled on the medial wall of the anterior ventral V-SVZ. The progenitors of type 1 cells were restricted to the very ventral tip of the medial wall (**Fig. 7c**), whereas type 3 cells were generated in a medial domain that did not appear to extend down to the tip of the lateral ventricle (**Fig. 7e**). By contrast, type 2 and type 4 cells were generated in a narrow domain restricted to the ventral tip of lateral V-SVZ (**Fig. 7d**,**f**). The spatial origin of type 1 and 3 cells largely overlapped with the Zic expression domain (**Fig. 7j**), supporting the hypothesis that Zic contributes to the specification of these cells.

Together, these findings suggest that the four new interneuron types that we identified are produced in distinct progenitor microdomains in the anterior ventral V-SVZ. These progenitor domains are quite small, extending only about 100–300 μm along the dorsal-ventral axis and 400–800 μm along the rostral-caudal axis (**Fig. 7c**–**f**) and collectively covering less than 5% of the surface area of the V-SVZ. Domains of this size would have been almost impossible

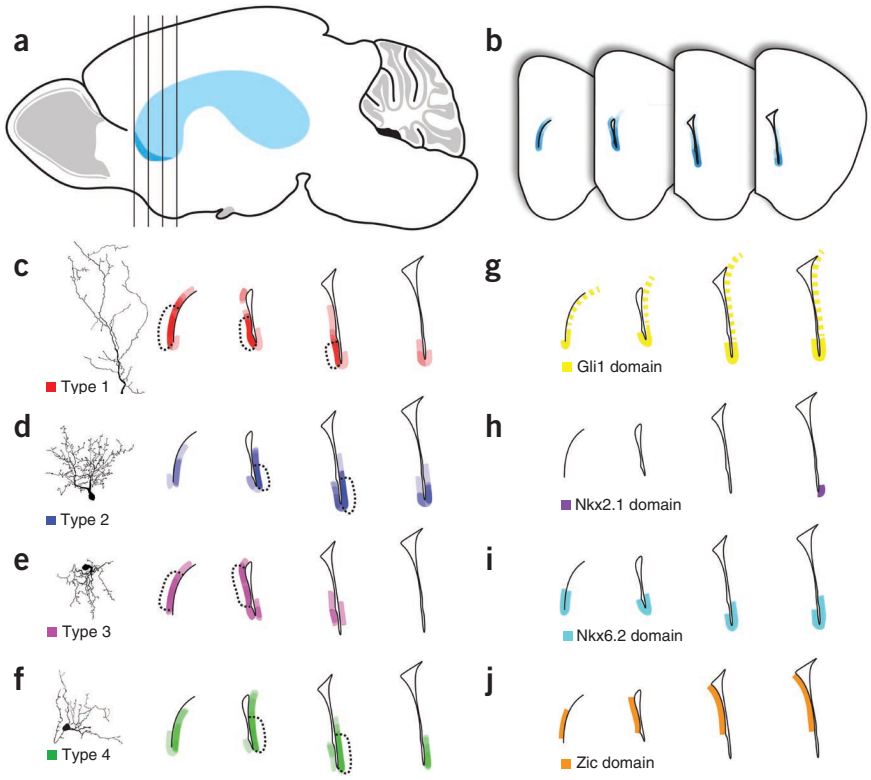

Figure 7 Type 1–4 cells are produced in distinct subregions of the anterior ventral V-SVZ. (**a**) Schematic lateral view of an adult mouse brain indicating the approximate spatial extent of the V-SVZ (light blue) including the subdomains that give rise to type 1–4 cells (dark blue). Vertical lines indicate the approximate regions from which the outline of the lateral ventricle is shown in coronal section in **b**–**j**. (**b**) Labeled V-SVZ regions (blue) of brains containing labeled type 1–4 cells were traced and overlaid onto a common template to reveal the origin of type 1–4 cells (dark blue). (**c**–**f**) This analysis was repeated for those brain regions giving rise to the highest percentage of type 1, 2, 3 or 4 cells, revealing a unique spatial origin for each of these cell types. Dotted lines define regions of highest overlap between injections. (**g**–**i**) Approximate spatial extent of the *Gli1* (**g**), *Nkx2.1* (**h**) and *Nkx6.2* (**i**) expression domains, as based on *CreER*^{T2} lineage tracing. Dashed line in **g** indicates lower expression. Nkx2.1 data in **h** are supported by immunostaining. (**j**) Approximate spatial extent of the Zic expression domain, as based on immunostaining (see also **Fig. 6** and **Supplementary Fig. 4**).

to discover without a combination of spatially restricted NSC targeting and gene marker analysis, which may explain why the postnatal production of type 1–4 cells has not been appreciated until now.

DISCUSSION

In this study, we systematically explored the complexity of progenitor domains in the postnatal mouse V-SVZ and identified adult progenitors in the anterior ventral V-SVZ that produce four novel types of OB interneuron. Here, we discuss the unique characteristics of the anterior ventral tip of the V-SVZ and the possible functions of type 1–4 neurons.

Developmental origin of the anterior ventral V-SVZ

The anterior ventral V-SVZ is located at the junction between the septum and the striatum, two regions that are derived from the embryonic septum and LGE, respectively[34]. The junctions of brain subregions are often sites of overlapping TF codes that specify distinct progenitor identities[8,34]. For example, the border of the LGE and the pallium is a region where pallial TFs such as Emx1 and Pax6 overlap with subpallial TFs such as Dlx1/2/5, Gsx1/2 (Gsh1/2) and Ascl1 (Mash1). This region of overlap defines the spatially limited domain where the TFs Sp8 and Dbx1 are expressed[12,34,46]. Similarly, the overlap of LGE TFs with the septal Zic TFs may define the Nkx6.2-positive progenitor domain in which type 1–4 cells are produced in the postnatal brain. Notably, Sp8 is also expressed in the septum[47], where it may contribute to the generation of CalR$^+$ type 1–4 cells.

The lineage relationship between OB neurons originating from common progenitor domains has not been described. For example, within the anterior ventral V-SVZ we observed the production of type 1 and 3 cells on the medial wall and type 2 and 4 cells on the lateral wall (**Fig. 7**). Similarly, superficial GCs and TH$^+$ PGCs are both produced in the dorsal and cortical V-SVZ, and deep GCs and CalB$^+$ PGCs are both produced in the ventral V-SVZ[9]. Therefore, progenitor domains generate different cell types. Whether these are generated by distinct progenitors with similar developmental histories or from common progenitors is unknown. This important problem could be addressed by clonal lineage tracing *in vivo*, where the potential of individual NSCs can be assessed.

Potential roles of type 1–4 interneurons in the OB circuitry

The continual addition and putative turnover of type 1–4 cells suggests that these cells are likely to be important in OB function. Based on their morphological properties and the existing literature, we speculate on how these four cell types may contribute to the function of the OB. The dendritic branches of deep-projecting GCs (type 1) in the granule cell layer and IPL position these cells to receive input from the axons of mitral and tufted cells and to inhibit the activity of projection neurons above them via their dendrites in the MCL and EPL. Shrub GCs (type 2) have spatially restricted, bushy arbors decorated with many spines that are concentrated near the proximal dendrites and cell bodies of mitral and tufted cells. The location of synapses on these cells close to the cell bodies of OB projection neurons suggests that these cells may mediate lateral inhibition. The extensive processes of PMCs (type 3) in the MCL and IPL suggest that they may interact with the cell bodies and axonal collaterals of mitral and tufted cells. The long, varicose processes of satellite cells (type 4) have previously been shown to associate with the dendrites of OB projection neurons, positioning them to inhibit broad stretches of mitral and tufted cell dendrites. A schematic diagram showing type 1–4 cells in relation to other OB cell types is given in **Supplementary Figure 6**.

While the functions of G_{IV}, G_V, PMC and satellite (type 1–4) cells are unclear, all of these cell types are generated postnatally, almost doubling the catalog of cell types known to be replaced in the adult brain. Furthermore, the spatial origin of these cells was restricted to a small region of the anterior ventral V-SVZ that was subdivided into progenitor microdomains at an unexpectedly fine level of organization, correlating well with the expression domains of Zic and Nkx6.2 TFs. This work extends the list of cell types replaced in the postnatal

brain and shows how interneuron diversity is achieved by the subdivision of the V-SVZ into distinct progenitor microdomains.

METHODS

Methods and any associated references are available in the online version of the paper.

Note: Any Supplementary Information and Source Data files are available in the online version of the paper.

ACKNOWLEDGMENTS

We would like to thank T. Nguyen, Z. Mirzadeh and R. Ihrie for comments and discussions that improved this study, and D. Rowitch (University of California, San Francisco) and R. Segal (Harvard Medical School) for generously sharing antibodies. R. Romero provided outstanding technical assistance with histology. M. Grist, U. Dennehy and M. Humphreys generated the *Nkx6.2::CreER^{T2}* transgenic mice, and *Gli1::CreER^{T2}* mice were generously provided by A. Joyner (Sloan-Kettering Institute). F.T.M. was supported by the US National Science Foundation, the Jane Coffin Childs Memorial Fund, the US National Institutes of Health (NIH) and the Harvard Stem Cell Institute. L.C.F. was supported by the Howard Hughes Medical Institute and the Helen Hay Whitney Foundation. This study was supported by grants from the NIH (HD 32116 and NS 28478), the John G. Bowes Research Fund, the European Research Council (207807) and the UK Medical Research Council (86419).

AUTHOR CONTRIBUTIONS

F.T.M., L.C.F. and A.A.-B. conceived and designed the experiments. F.T.M., L.C.F., T.A.S. and L.M. conducted experiments. N.K. developed the *Nkx6.2CreER^{T2}* transgenic mice and critically reviewed and edited the manuscript. F.T.M., L.C.F. and A.A.-B. analyzed data and prepared the manuscript. F.T.M. wrote the manuscript.

COMPETING FINANCIAL INTERESTS

The authors declare no competing financial interests.

1. Alvarez-Buylla, A. & Garcia-Verdugo, J.M. Neurogenesis in adult subventricular zone. *J. Neurosci.* **22**, 629–634 (2002).
2. Sakamoto, M. *et al.* Continuous neurogenesis in the adult forebrain is required for innate olfactory responses. *Proc. Natl. Acad. Sci. USA* **108**, 8479–8484 (2011).
3. Imayoshi, I. *et al.* Roles of continuous neurogenesis in the structural and functional integrity of the adult forebrain. *Nat. Neurosci.* **11**, 1153–1161 (2008).
4. Kosaka, K. *et al.* Chemically defined neuron groups and their subpopulations in the glomerular layer of the rat main olfactory bulb. *Neurosci. Res.* **23**, 73–88 (1995).
5. Price, J.L. & Powell, T.P. The mitral and short axon cells of the olfactory bulb. *J. Cell Sci.* **7**, 631–651 (1970).
6. Shepherd, G.M. *The Synaptic Organization of the Brain* (Oxford Univ. Press, 2004).
7. Doetsch, F., Caille, I., Lim, D.A., Garcia-Verdugo, J.M. & Alvarez-Buylla, A. Subventricular zone astrocytes are neural stem cells in the adult mammalian brain. *Cell* **97**, 703–716 (1999).
8. Alvarez-Buylla, A., Kohwi, M., Nguyen, T.M. & Merkle, F.T. The heterogeneity of adult neural stem cells and the emerging complexity of their niche. *Cold Spring Harb. Symp. Quant. Biol.* **73**, 357–365 (2008).
9. Merkle, F.T., Mirzadeh, Z. & Alvarez-Buylla, A. Mosaic organization of neural stem cells in the adult brain. *Science* **317**, 381–384 (2007).
10. Kelsch, W., Mosley, C.P., Lin, C.-W. & Lois, C. Distinct mammalian precursors are committed to generate neurons with defined dendritic projection patterns. *PLoS Biol.* **5**, e300 (2007).
11. Ventura, R.E. & Goldman, J.E. Dorsal radial glia generate olfactory bulb interneurons in the postnatal murine brain. *J. Neurosci.* **27**, 4297–4302 (2007).
12. Young, K.M., Fogarty, M., Kessaris, N. & Richardson, W.D. Subventricular zone stem cells are heterogeneous with respect to their embryonic origins and neurogenic fates in the adult olfactory bulb. *J. Neurosci.* **27**, 8286–8296 (2007).
13. Kriegstein, A. & Alvarez-Buylla, A. The glial nature of embryonic and adult neural stem cells. *Annu. Rev. Neurosci.* **32**, 149–184 (2009).
14. Novak, A., Guo, C., Yang, W., Nagy, A. & Lobe, C.G. Z/EG, a double reporter mouse line that expresses enhanced green fluorescent protein upon Cre-mediated excision. *Genesis* **28**, 147–155 (2000).
15. Seri, B. *et al.* Composition and organization of the SCZ: a large germinal layer containing neural stem cells in the adult mammalian brain. *Cereb. Cortex* **16** (suppl. 1), i103–i111 (2006).
16. Kohwi, M. *et al.* A subpopulation of olfactory bulb GABAergic interneurons is derived from Emx1- and Dlx5/6-expressing progenitors. *J. Neurosci.* **27**, 6878–6891 (2007).
17. Alonso, M. *et al.* Turning astrocytes from the rostral migratory stream into neurons: a role for the olfactory sensory organ. *J. Neurosci.* **28**, 11089–11102 (2008).
18. Mirzadeh, Z., Merkle, F.T., Soriano-Navarro, M., Garcia-Verdugo, J.M. & Alvarez-Buylla, A. Neural stem cells confer unique pinwheel architecture to the ventricular surface in neurogenic regions of the adult brain. *Cell Stem Cell* **3**, 265–278 (2008).
19. Shepherd, G., Chen, W., Willhite, D., Migliore, M. & Greer, C. The olfactory granule cell: from classical enigma to central role in olfactory processing. *Brain Res. Brain Res. Rev.* **55**, 373–382 (2007).
20. Schneider, S.P. & Macrides, F. Laminar distributions of interneurons in main olfactory-bulb of adult hamster. *Brain Res. Bull.* **3**, 73–82 (1978).
21. Mori, K., Kishi, K. & Ojima, H. Distribution of dendrites of mitral, displaced mitral, tufted, and granule cells in the rabbit olfactory-bulb. *J. Comp. Neurol.* **219**, 339–355 (1983).
22. Blanes, T. Sobre algunos puntos dudosos de la estrucutra del bulbo olfactario. *Revista Trimestral Micrografica* **3**, 99–127 (1898).
23. Shepherd, G.M. Synaptic organization of the mammalian olfactory bulb. *Physiol. Rev.* **52**, 864–917 (1972).
24. López-Mascaraque, L., De Carlos, J.A. & Valverde, F. Structure of the olfactory bulb of the hedgehog (*Erinaceus europaeus*): a Golgi study of the intrinsic organization of the superficial layers. *J. Comp. Neurol.* **301**, 243–261 (1990).
25. Larriva-Sahd, J. The accessory olfactory bulb in the adult rat: a cytological study of its cell types, neuropil, neuronal modules, and interactions with the main olfactory system. *J. Comp. Neurol.* **510**, 309–350 (2008).
26. Van Gehuchten, A.I.M. Le bulbe olfactif chez quelques mammiferes. *Cellule* **5**, 205–237 (1891).
27. Ihrie, R.A. *et al.* Persistent sonic hedgehog signaling in adult brain determines neural stem cell positional identity. *Neuron* **71**, 250–262 (2011).
28. Ahn, S. & Joyner, A.L. Dynamic changes in the response of cells to positive hedgehog signaling during mouse limb patterning. *Cell* **118**, 505–516 (2004).
29. Danielian, P.S., Muccino, D., Rowitch, D.H., Michael, S.K. & McMahon, A.P. Modification of gene activity in mouse embryos in utero by a tamoxifen-inducible form of Cre recombinase. *Curr. Biol.* **8**, 1323–1326 (1998).
30. Mao, J. *et al.* A novel somatic mouse model to survey tumorigenic potential applied to the Hedgehog pathway. *Cancer Res.* **66**, 10171–10178 (2006).
31. Price, M. Members of the Dlx- and Nkx2-gene families are regionally expressed in the developing forebrain. *J. Neurobiol.* **24**, 1385–1399 (1993).
32. Sussel, L., Marin, O., Kimura, S. & Rubenstein, J.L. Loss of Nkx2.1 homeobox gene function results in a ventral to dorsal molecular respecification within the basal telencephalon: evidence for a transformation of the pallidum into the striatum. *Development* **126**, 3359–3370 (1999).
33. Marin, O., Anderson, S.A. & Rubenstein, J.L. Origin and molecular specification of striatal interneurons. *J. Neurosci.* **20**, 6063–6076 (2000).
34. Flames, N. *et al.* Delineation of multiple subpallial progenitor domains by the combinatorial expression of transcriptional codes. *J. Neurosci.* **27**, 9682–9695 (2007).
35. Taniguchi, H., Lu, J. & Huang, Z.J. The spatial and temporal origin of chandelier cells in mouse neocortex. *Science* **339**, 70–74 (2013).
36. Magno, L., Catanzariti, V., Nitsch, R., Krude, H. & Naumann, T. Ongoing expression of Nkx2.1 in the postnatal mouse forebrain: potential for understanding NKX2.1 haploinsufficiency in humans? *Brain Res.* **1304**, 164–186 (2009).
37. Xu, Q., Tam, M. & Anderson, S.A. Fate mapping Nkx2.1-lineage cells in the mouse telencephalon. *J. Comp. Neurol.* **506**, 16–29 (2008).
38. Tsai, H.-H. *et al.* Regional astrocyte allocation regulates CNS synaptogenesis and repair. *Science* doi:10.1126/science.1222381 (2012).
39. Inan, M., Welagen, J. & Anderson, S.A. Spatial and temporal bias in the mitotic origins of somatostatin- and parvalbumin-expressing interneuron subgroups and the chandelier subtype in the medial ganglionic eminence. *Cereb. Cortex* **22**, 820–827 (2012).
40. Moreno-Bravo, J.A., Perez-Balaguer, A., Martinez, S. & Puelles, E. Dynamic expression patterns of Nkx6.1 and Nkx6.2 in the developing mes-diencephalic basal plate. *Dev. Dyn.* **239**, 2094–2101 (2010).
41. Inoue, T., Ota, M., Ogawa, M., Mikoshiba, K. & Aruga, J. Zic1 and Zic3 regulate medial forebrain development through expansion of neuronal progenitors. *J. Neurosci.* **27**, 5461–5473 (2007).
42. Aruga, J. *et al.* A novel zinc finger protein, zic, is involved in neurogenesis, especially in the cell lineage of cerebellar granule cells. *J. Neurochem.* **63**, 1880–1890 (1994).
43. Wataya, T. *et al.* Minimization of exogenous signals in ES cell culture induces rostral hypothalamic differentiation. *Proc. Natl. Acad. Sci. USA* **105**, 11796–11801 (2008).
44. Borghesani, P.R. *et al.* BDNF stimulates migration of cerebellar granule cells. *Development* **129**, 1435–1442 (2002).
45. Doetsch, F., Garcia-Verdugo, J.M. & Alvarez-Buylla, A. Cellular composition and three-dimensional organization of the subventricular germinal zone in the adult mammalian brain. *J. Neurosci.* **17**, 5046–5061 (1997).
46. Puelles, L. *et al.* Pallial and subpallial derivatives in the embryonic chick and mouse telencephalon, traced by the expression of the genes Dlx-2, Emx-1, Nkx-2.1, Pax-6, and Tbr-1. *J. Comp. Neurol.* **424**, 409–438 (2000).
47. Waclaw, R.R. *et al.* The zinc finger transcription factor sp8 regulates the generation and diversity of olfactory bulb interneurons. *Neuron* **49**, 503–516 (2006).

ONLINE METHODS

Neural stem cell targeting. All animal procedures were carried out in accordance with institutional (IACUC) and NIH guidelines. NSCs were targeted by injection of Cre-expressing adenovirus (Ad:Cre or Ad:GFAP-Cre) into Z/EG reporter mice as previously described[9].

Perfusion and immunohistochemistry. Mice were sacrificed and their brains were processed for immunohistochemistry as previously described[9]. Antibodies used are given in **Supplementary Table 1**. Biotin-conjugated antibodies were visualized by ABC reaction (Vector) followed by diaminobenzidine (DAB) with or without nickel.

Generation of Nkx6.2-CreERT2 transgenic mice. Mice expressing CreER^{T2} under control of the *Nkx6.2* gene were generated using bacterial artificial chromosome (BAC) transgenic technology as previously described[48]. A codon-improved iCreER^{T2} recombinase was fused to the initiation codon of the *Nkx6.2* gene using a PCR-based approach. A simian virus 40 polyadenylation signal was inserted at a position immediately after the ATG-encoding exon of *Nkx6.2* (**Supplementary Fig. 3**). BAC modification was performed in a bacterial system as described previously[49].

Identification and region of origin analysis of novel cell types. To determine the V-SVZ regions where type 1–4 cells were produced, we traced coronal brain sections from the Allen Brain Reference Atlas (http://mouse.brain-map.org/experiment/thumbnails/100048576?image_type=atlas) in Adobe Illustrator CS (Adobe Systems Inc.) at approximately 200-μm increments from the OB (coronal level 26, bregma 4.845 mm) to bregma (coronal level 54, bregma 0.020 mm). Next we digitally painted the V-SVZ regions containing labeled progenitors onto these traces and overlaid them in Illustrator. We selected the ten hemispheres with the largest percentage of type 1 cells relative to other labeled OB cell types (**Fig. 7c**) and overlaid the traces of labeled V-SVZ cells (red) to identify regions in which at least half (five of ten) of the traces overlapped (dotted line), to identify likely progenitor domains for each cell type. This analysis was repeated for type 2–4 cells (**Fig. 7d–f**).

Imaging and camera lucida tracing. DAB-labeled cells were studied on an Olympus AX70 microscope with a Retiga 2000R digital camera (Qimaging Corporation) and processed using Openlab 5.0.1 (Improvision Inc.). Fluorescence images of immunostained brain sections were taken on a Leica TCS SP5 confocal microscope using the Leica LAS AF imaging software. Images were processed for brightness and contrast using Adobe Photoshop CS (Adobe Systems Inc.). We manually quantified double-labeled cells at 40–100× magnification on an Olympus AX70 microscope. For marker gene analysis, we counted a minimum of 30 different type 1–4 cells from at least three separate injections. For camera lucida tracing, we selected at least 10 representative DAB-immunostained type 1–4 cells that had largely intact dendritic arbors with a mature morphology (branched and spine-bearing). We traced only cells that were physically separated from other labeled cells. In **Supplementary Figure 4**, brain sections and GFP$^+$ cells were mapped using Neurolucida (v10.54, MBF Biosciences-MicroBrightField Inc.).

Morphological analysis. For morphological analysis, at least 20 immunoperoxidase-labeled cells of each type (type 1–4) were studied using ImageJ software (NIH). To calculate the position of the cell in the OB, we measured its radial distance from the center of the MCL and divided this measurement by the radial distance from the OB core to the top of the EPL (bottom of the GL). Similarly, we measured the distance from the center of the MCL to the tip of the most superficial dendrite for each cell type and normalized this distance to the thickness of the EPL. To quantify dendritic branching, the primary dendrite was defined as the longest and largest diameter neurite emanating from the soma. Secondary dendrites were defined as processes that radiated from this primary dendrite and tertiary dendrites as processes directly connected to secondary dendrites. Quantifications and number of cells analyzed are provided in the Source Data.

48. Fogarty, M. *et al.* Spatial genetic patterning of the embryonic neuroepithelium generates GABAergic interneuron diversity in the adult cortex. *J. Neurosci.* **27**, 10935–10946 (2007).
49. Lee, E.C. *et al.* A highly efficient *Escherichia coli*-based chromosome engineering system adapted for recombinogenic targeting and subcloning of BAC DNA. *Genomics* **73**, 56–65 (2001).